Performance Analysis of Wireless Systems With Doubly Selective Rayleigh Fading

Jingxian Wu, *Member, IEEE*, and Chengshan Xiao, *Senior Member, IEEE*

***Abstract*—Theoretical error performances of wireless communication systems suffering from both doubly selective (time varying and frequency selective) Rayleigh fading and sampler timing offset are analyzed in this paper. Single-input–single-output systems with doubly selective fading channels are equivalently represented as discrete-time single-input–multiple-output (SIMO) systems with *correlated* frequency-flat fading channels, with the correlation information being determined by the combined effects of sampler timing phase, maximum Doppler spread, and power delay profile of the physical fading. Based on the equivalent SIMO system representation, closed-form error-probability expressions are derived as tight lower bounds for linearly modulated systems with fractionally spaced equalizers. The information on the sampler timing offset and the statistical properties of the physical channel fading, along with the effects of the fractionally spaced equalizer, are incorporated in the error-probability expressions. Simulation results show that the new analytical results can accurately predict the error performances of maximum-likelihood sequence estimation and maximum *a posteriori* equalizers for practical wireless communication systems in a wide range of signal-to-noise ratio. Moreover, some interesting observations about receiver oversampling and system timing phase sensitivity are obtained based on the new analytical results.**

***Index Terms*—Doubly selective fading, error performance, fractionally spaced equalizer, power delay profile (PDP), sensitivity, timing phase.**

I. Introduction

PERFORMANCE analysis of wireless communication systems experiencing frequency-selective fading has been a field of interest for a long time, e.g., see [1]–[15] and the references therein. One of the most popular analytical methods used for performance analysis of systems with frequency-selective fading channels (or other trellis structured systems) is the union-bound technique [1]–[8], with which system performance upper bounds are evaluated by summing over pairwise error probabilities (PEPs) of mutually overlapped error events. Based on the methods used for the computation of the error events PEP, the union bounds are classified as the union Chernoff bound and the true union bound (TUB) in [8].

Most of the union-bound results are for systems with symbol-spaced equalizers, i.e., the sampling period T_s at the receiver is equal to the system symbol period $T_{\rm sym}$. It is well known that the performance of symbol-spaced systems depends critically on the sampler timing phase [16], [17]. The timing phase sensitivity of symbol-spaced equalizers is induced by the effects of spectrum aliasing of the sampled signals, and it can be avoided by the implementation of fractionally spaced equalizers with $T_s < T_{\rm sym}$ [17]. The design and union bounds of a fractionally spaced receiver with maximum-likelihood sequence estimation (MLSE) equalizers are briefly discussed in [4]. The union-bound technique provides an effective way to evaluate the upper bounds of system performances. However, the results obtained with the union bound are very loose, and the bounds usually diverge at low SNR.

Matched filter bounds are derived in [9]–[14] by assuming that ideal equalization is available at the receiver and that the receive filter is perfectly matched to the composite impulse response (CIR) of the transmit filter and the channel fading. The matched filter bound for a simple two-ray fading channel is analyzed in [9], and systems with general power delay profiles (PDPs) are discussed in [10] and [13] with the help of frequency-domain analysis and Karhunen–Loève expansion. With ideal receiver assumptions, the matched filter bound defines the best performance that may be achieved under a certain system configuration, whereas it is usually far below the actual error performances of systems with practical receivers.

In this paper, error performance analysis is carried out for systems with doubly selective Rayleigh fading channels and practical system configurations. New tight closed-form error performance lower bounds are derived for linearly modulated systems with both symbol-spaced equalizers and fractionally spaced equalizers. The combined effects of the transmit filter, receive filter, and the physical doubly selective fading are represented as a sampling interval spaced discrete-time tapped-delay-line filter with *correlated* tap coefficients, with the correlation information being determined by the sampler timing phase, maximum Doppler spread, and PDP of the physical channel fading.

Instead of resorting to the complex trellis structure analysis utilized in the union-bound technique, the new performance bound is evaluated on a sample-by-sample basis with an equivalent single-input–multiple-output (SIMO) system method, where single-input–single-output (SISO) communication systems with doubly selective fading channels and additive white Gaussian noise (AWGN) are equivalently represented as SIMO systems with mutually correlated frequency-flat fading channels and colored Gaussian noise, with the noise correlation introduced by the time span of the receive filter and receiver oversampling [18]. Compared to the frequency-domain analysis

Manuscript received May 16, 2005; revised February 1, 2006 and April 21, 2006. This work was supported in part by the National Science Foundation under Grant CCF-0514770 and by the University of Missouri-Columbia Research Council under Grant URC-05-064. The review of this paper was coordinated by Dr. A. Chockalingam.

J. Wu is with the Department of Engineering Science, Sonoma State University, Rohnert Park, CA 94928 USA (e-mail: jingxian.wu@sonoma.edu).

C. Xiao is with the Department of Electrical and Computer Engineering, University of Missouri, Columbia, MO 65211 USA (e-mail: xiaoc@missouri.edu).

Digital Object Identifier 10.1109/TVT.2007.891438

utilized by the matched filter bound [10], a much simpler time-domain analysis is employed in the derivation of the new bounds. It is shown by simulations that our new analytical results can accurately predict the error performances of maximum *a posteriori* (MAP) and MLSE equalizers at both low SNR and high SNR. Moreover, it is observed in this paper that for systems with practical PDPs, a fractionally spaced equalizer cannot only overcome the problem of timing phase sensitivity but can also achieve significant performance gain over systems with symbol-spaced receivers.

The rest of this paper is organized as follows: Section II presents a discrete-time representation of the communication systems experiencing doubly selective fading, and the statistical properties of the discrete-time system model are analyzed. In Section III, an equivalent SIMO system representation is presented to facilitate error performance analysis. Based on an optimum decision rule proposed for the equivalent SIMO system, closed-form expressions of the new error-probability bounds for a system with doubly selective fading channels are derived in Section IV. Numerical examples and simulation results are given in Section V, and Section VI concludes this paper.

II. Discrete-Time System Model

An equivalent discrete-time system model is derived in this section for systems experiencing time-varying and frequency-selective channel fading.

Let $p_T(t)$ and $p_R(t)$ be the time-invariant impulse response of the transmit filter and receive filter, respectively, where both are normalized with energy of unity. Let $g(t,\tau)$ be the time-varying impulse response of the doubly selective fading channel, and it can be viewed as the response of the fading channel at time t to an impulse input applied at time $t-\tau$. We define the continuous-time CIR of the channel as follows:

$$h_c(t,\tau) = p_R(\tau) \circledast g(t,\tau) \circledast p_T(\tau) \tag{1}$$

where

$$a(\tau) \circledast b(t,\tau) = \int_{-\infty}^{+\infty} a(\mu) b(t-\mu, \tau-\mu) d\mu \tag{2a}$$

$$a(t,\tau) \circledast b(\tau) = \int_{-\infty}^{+\infty} a(t,\mu) b(\tau-\mu) d\mu \tag{2b}$$

represent the convolution operation of time-varying systems. Therefore, the signal at the receiver $y_c(t)$ can be represented by

$$y_c(t) = \sum_{n=-\infty}^{+\infty} s(n) h_c(t, t-nT_{\rm sym}) + z_c(t) \tag{3}$$

where $s(n)$ is the modulated information symbol with symbol period $T_{\rm sym}$, $z_c(t) = p_R(t) \circledast v_c(t)$ is the noise component at the output of the receive filter, and $v_c(t)$ is the zero-mean complex-valued white Gaussian noise with variance N_0. The sampled output of the receive filter at the sampling instant $kT_s + \tau_0$ can be expressed by

$$y(k) = \sum_{l=0}^{L-1} x(k-l) h(k,l) + z(k) \tag{4}$$

where the sampling period T_s satisfies $T_s = T_{\rm sym}/\nu$, with the integer ν being the oversampling factor; L is the channel length of the composite channel; $\tau_0 \in [-(T_s/2), (T_s/2)]$ is the sampler timing offset; $y(k) = y_c(kT_s + \tau_0)$ and $z(k) = z_c(kT_s + \tau_0)$ are the time-shifted T_s-spaced samples of the received signals and noise components, respectively; $h(k,n) = h_c(kT_s + \tau_0, nT_s + \tau_0)$ is the sampled version of the continuous-time CIR $h_c(t,\tau)$; and $x(k)$ is the oversampled version of the transmitted signals $s(k)$ defined as

$$x(k) = \begin{cases} s(k/\nu), & k/\nu \text{ is integer} \\ 0, & \text{otherwise.} \end{cases}$$

In the representation of (4), the CIR $h(k,l)$ is represented as a causal finite-impulse response (FIR) filter in the delay domain l by discarding negligible channel taps. This FIR representation can be verified by the facts that the PDP $G(\mu)$ of the physical fading channel has finite-time-domain support, and the tails of the transmit filter and receive filter fall off rapidly in the time domain. Moreover, systems with noncausal CIR can always be made causal by appropriate delays at the receiver.

Equation (4) is a discrete-time representation of the communication system, and the doubly selective fading channel is represented as a T_s-spaced tapped-delay-line filter. It is shown in [18] that the tap coefficients of $h(k,l)$ are mutually correlated in both temporal domain k and delay domain l. If the channel experiences wide sense stationary uncorrelated scattering (WSSUS) Rayleigh fading, then the correlation function $\rho(k_1 - k_2; l_1, l_2) = E[h(k_1, l_1) h^*(k_2, l_2)]$ can be expressed by [18]

$$\rho(k_1 - k_2; l_1, l_2) = J_0\left[2\pi f_d (k_1 - k_2) T_s\right] \cdot c(l_1, l_2) \tag{5}$$

with

$$c(l_1, l_2) = \int_{-\infty}^{+\infty} R_{p_T p_R}(l_1 T_s + \tau_0 - \mu) \cdot R^*_{p_T p_R}(l_2 T_s + \tau_0 - \mu) G(\mu) d\mu \tag{6}$$

where $R_{p_T p_R}(t) = p_T(t) \circledast p_R(t)$ is the convolution of the transmit filter and receive filter, $J_0(x)$ is the zero-order Bessel function of the first kind, f_d is the maximum Doppler spread of the channel fading, and $G(\mu)$ is the normalized channel PDP with $\int_{-\infty}^{+\infty} G(\mu) d\mu = 1$. It needs to be pointed out [19] that (5) holds for the condition that $f_d T_s \ll 1$, which is satisfied for most practical conditions. The delay domain correlation $c(l_1, l_2)$ of the discrete-time CIR is introduced by the effects of the time span of the filters $p_T(t)$ and $p_R(t)$, whereas the underlying WSSUS physical fading channels are uncorrelated in the delay domain τ. As defined in (5) and (6), the values of the temporal-delay 2-D correlation $\rho(k; l_1, l_2)$ are jointly

determined by the maximum Doppler spread f_d, the PDP $G(\mu)$ of the physical channel fading, the sampler timing offset τ_0, and the effects of the transmit filter $p_T(t)$ and receive filter $p_R(t)$.

The noise component $z(k)$ of the discrete-time system is a linear transformation of the AWGN $v(t)$; thus, it is still Gaussian distributed with zero mean, and the autocorrelation function is given by [18]

$$E\left[z(m+n)z^*(m)\right] = N_0 \cdot R_{p_R p_R}(nT_s) \tag{7}$$

where $R_{p_R p_R}(nT_s) = \int_{-\infty}^{+\infty} p_R(nT_s+\tau)p_R(\tau)d\tau$ is the autocorrelation function of the receive filter. It should be noted that the statistical properties of the noise component are not affected by the timing offset τ_0. If $R_{p_R p_R}(nT_s) = 0$ for $n \neq 0$, then the discrete-time noise component $z(k)$ is still white, and this is valid for T_{sym}-spaced receivers with Nyquist filter. For fractionally spaced receivers, $z(k)$ becomes a colored Gaussian noise process, and the correlation among noise samples is introduced by the effects of oversampling and the time span of the receive filter. It will be shown in this paper that the temporal-delay correlation information of $h(k,l)$ along with the noise correlation is critical to the performances of the communication systems.

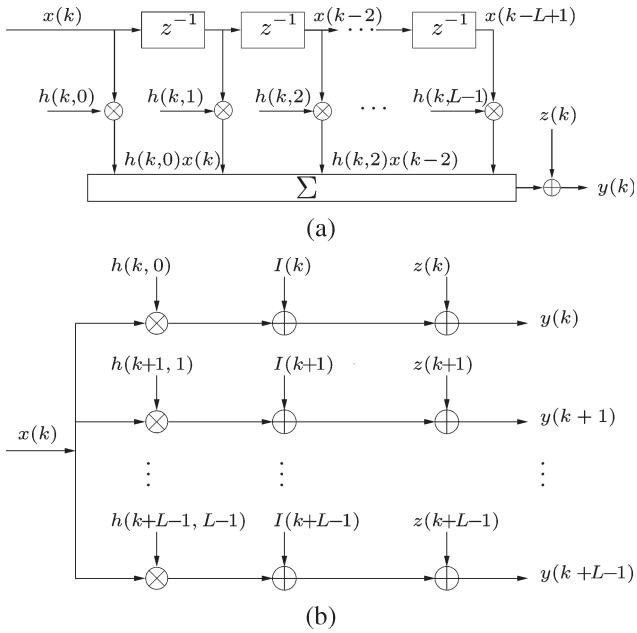

Fig. 1. Block diagrams of the SISO system and its equivalent SIMO system representation. (a) Discrete-time SISO system with doubly selective fading channel. (b) Equivalent SIMO system representation.

III. Equivalent System Representation

An equivalent SIMO representation of a system with doubly selective channel fading is presented in this section to facilitate system error performance analysis.

Based on the discrete-time representation of the system given in (4), the input–output relationship of the system can be written in matrix format as

$$\mathbf{y}_k = \mathbf{h}_k \cdot x(k) + \widetilde{\mathbf{H}}_k \cdot \tilde{\mathbf{x}}_k + \mathbf{z}_k \tag{8}$$

where the vectors $\mathbf{y}_k = [y(k), y(k+1), \ldots, y(k+L-1)]^T \in \mathbb{C}^{L\times 1}$; $\mathbf{z}(k) = [z(k), z(k+1), \ldots, z(k+L-1)]^T \in \mathbb{C}^{L\times 1}$ comprise all the received samples and noise samples related to the transmitted symbol $x(k)$, with $\mathbf{A}^T$ representing the operation of matrix transpose; $\mathbf{h}_k = [h(k,0), h(k+1,1), \ldots, h(k+L-1, L-1)]^T \in \mathbb{C}^{L\times 1}$ is the CIR vector related to $x(k)$; $\tilde{\mathbf{x}}_k = [x(k-L+1), \ldots, x(k-1), x(k+1), \ldots, x(k+L-1)]^T \in \mathbb{C}^{2(L-1)\times 1}$ is the interference vector relative to $x(k)$; and $\widetilde{\mathbf{H}}_k$ is the corresponding interference CIR matrix defined by (9), shown at the bottom of the page.

In the representation of (8), $x(k)$ is treated as the desired information symbol being transmitted in L parallel frequency-flat fading channels, and the SISO system with doubly selective fading channel is equivalently represented as a SIMO system with L mutually correlated flat fading channels $\mathbf{h}_k$ and colored additive noise $\mathbf{z}_k$. The ISI components $\mathbf{I}_k = \widetilde{\mathbf{H}}_k\tilde{\mathbf{x}}_k = [I(k), I(k+1), \ldots, I(k+L-1)]^T$ are represented as additive interferences arising from channel components that are irrelevant to the detection of the desired symbol $x(k)$. The block diagrams of the original SISO system along with its SIMO counterpart are depicted in Fig. 1. With such system configurations, the system error performances can be analyzed on a samplewise basis without resorting to the trellis structure utilized by union-bound techniques. Moreover, we are going to show by simulations that the results obtained by this method are more accurate than those obtained from union bound and matched filter bound.

If the interference components, i.e., $\mathbf{I}_k = \widetilde{\mathbf{H}}_k\tilde{\mathbf{x}}_k$, are fully canceled by the receiver, then the minimum error probability of the SIMO system can be achieved through optimum combining performed over the L correlated flat fading channels. It is well known that MLSE equalizers and MAP equalizers are optimum in the sense of maximizing the likelihood functions or *a posteriori* probabilities of the transmitted symbols. In this paper, we are going to show by simulations that the MLSE and MAP equalizers are also asymptotically optimum for the equivalent SIMO systems in the sense of interference cancellation, i.e., if MAP or MLSE equalization algorithms are employed at the receiver, the interference components $\mathbf{I}_k$ at the output of the equalizers will tend to 0 when the SNR tends to infinity. Therefore, the tight error-probability lower bounds of MLSE and MAP equalizers can be obtained by assuming $\mathbf{I}_k = 0$.

$$\widetilde{\mathbf{H}}_k = \begin{bmatrix} h(k,L-1) & \cdots & h(k,1) & 0 & \cdots & 0 \\ 0 & h(k+1,L-1) & \cdots & h(k+1,2) & h(k+1,0) & 0 \\ \vdots & \vdots & \vdots & \vdots & \vdots & \vdots \\ 0 & \cdots & 0 & h(k+L-1,L-2) & \cdots & h(k+L-1,0) \end{bmatrix} \in \mathbb{C}^{L\times 2(L-1)} \tag{9}$$

It is worth pointing out that the interference-free assumption is also employed in the derivation of the matched filter bounds [9]–[14], where ideal lower bounds are obtained by assuming that the receive filter is perfectly matched to the combined response of the transmit filter and channel fading. The ideal receiver assumption makes the matched filter bounds unachievable for most practical systems. On the other hand, by considering the effects of practical receive filter and sampler timing phase, the error performance bounds obtained by the equivalent SIMO system method can accurately predict the performance of systems with practical equalizers.

From (8), the interference-free SIMO system can be represented as

$$\mathbf{y}_k = \mathbf{h}_k \cdot x(k) + \mathbf{z}_k \tag{10}$$

where $\mathbf{z}_k$ is a zero-mean colored Gaussian noise vector. The correlation among the noise samples is introduced by the time span of the receive filter, as expressed in (7), and the covariance matrix of $\mathbf{z}_k$ is $\mathbf{R}_z = E[\mathbf{z}_k \mathbf{z}_k^H] = N_0 \cdot \mathbf{R}_p$, where $\mathbf{A}^H$ denotes the matrix Hermitian operation, and $\mathbf{R}_p$ is the receive filter correlation matrix defined by (11), shown at the bottom of the page.

The Rayleigh fading channel vector $\mathbf{h}_k$ contains zero-mean complex Gaussian random variables (CGRVs) with covariance matrix $\mathbf{R}_h = E[\mathbf{h}_k \mathbf{h}_k^H]$ given by (12), shown at bottom of the page.

The correlation coefficient $\rho(k; l_1, l_2)$ is defined in (5), and it contains the information of both the temporal correlation $J_0(2\pi f_d k T_s)$ and the delay domain correlation $c(l_1, l_2)$, which are in turn determined by the maximum Doppler spread f_d, the sampler timing offset τ_0, and the PDP $G(\mu)$ of the channel fading.

Based on the statistical properties of the noise vector $\mathbf{z}_k$ and the CIR vector $\mathbf{h}_k$, the error probabilities of the communication system are analyzed in the next section.

IV. Error Performance Analysis

Closed-form expressions of the symbol error rate (SER) of linearly modulated systems are derived based on an optimum decision rule for the interference-free SIMO system. SERs obtained by this method are the tight lower performance bounds of the corresponding SISO system.

A. Conditional Error Probability

The conditional error probability of linearly modulated system is derived in this section based on an optimum decision rule proposed for the interference-free SIMO system with colored Gaussian noise.

For the oversampled system, the noise covariance matrix $\mathbf{R}_z = N_0 \mathbf{R}_p$ might be rank deficient. To facilitate analysis, we resort to the pseudoinverse of receive filter correlation matrix $\mathbf{R}_p$. The corresponding pseudoinverse matrix $\mathbf{\Psi}_p$ can be written as

$$\mathbf{\Psi}_p = \mathbf{V} \mathbf{\Omega}_p^{-1} \mathbf{V}^H \in \mathbb{C}^{L \times L} \tag{13}$$

with

$$\mathbf{V} = [\mathbf{v}_1 \quad \mathbf{v}_2 \quad \cdots \quad \mathbf{v}_{L_p}] \in \mathbb{C}^{L \times L_p} \tag{14a}$$

$$\mathbf{\Omega}_p = \mathrm{diag}[\omega_1 \quad \omega_2 \quad \cdots \quad \omega_{L_p}] \in \mathbb{R}^{L_p \times L_p} \tag{14b}$$

where L_p is the number of nonzero eigenvalues of $\mathbf{R}_p$, $\mathbf{\Omega}_p$ is a diagonal matrix with its diagonal elements being the nonzero eigenvalues of $\mathbf{R}_p$, and the corresponding orthonormal eigenvectors $\mathbf{v}_l$, for $l = 1, 2, \ldots, L_p$, form the reduced eigenvector matrix $\mathbf{V}$.

With the pseudoinverse matrix $\mathbf{\Psi}_p$ given in (13), we can define the noise whitening matrix of the SIMO system as $\mathbf{W} = \mathbf{V} \Omega_p^{-1/2} \in \mathbb{C}^{L \times L_p}$. Applying $\mathbf{W}^H$ to both sides of the SIMO system defined in (10), we have an equivalent system

$$\bar{\mathbf{y}}_k = \bar{\mathbf{h}}_k \cdot x(k) + \bar{\mathbf{z}}_k \tag{15}$$

where $\bar{\mathbf{y}}_k = \mathbf{W}^H \mathbf{y}_k$, $\bar{\mathbf{h}}_k = \mathbf{W}^H \mathbf{h}_k$, and $\bar{\mathbf{z}}_k = \mathbf{W}^H \mathbf{z}_k$ are the sample vector, channel vector, and noise vector of the equivalent system, respectively. The noise vector $\bar{\mathbf{z}}_k$ is obtained from the linear transformation of the colored Gaussian vector $\mathbf{z}_k \sim \mathcal{N}(\mathbf{0}, N_0 \mathbf{R}_p)$; thus, $\bar{\mathbf{z}}_k$ is still Gaussian distributed with zero mean. The covariance matrix $\mathbf{R}_{\bar{z}} = E[\bar{\mathbf{z}}_k \bar{\mathbf{z}}_k^H]$ of $\bar{\mathbf{z}}_k$ is

$$\mathbf{R}_{\bar{z}} = \mathbf{W}^H \mathbf{R}_z \mathbf{W} = N_0 \cdot \mathbf{I}_{L_p} \tag{16}$$

$$\mathbf{R}_p = \begin{bmatrix} R_{p_R p_R}(0) & R_{p_R p_R}(T_s) & \cdots & R_{p_R p_R}[(L-1)T_s] \\ R_{p_R p_R}(T_s) & R_{p_R p_R}(0) & \cdots & R_{p_R p_R}[(L-2)T_s] \\ \vdots & \vdots & \vdots & \vdots \\ R_{p_R p_R}[(L-1)T_s] & R_{p_R p_R}[(L-2)T_s] & \cdots & R_{p_R p_R}(0) \end{bmatrix} \tag{11}$$

$$\mathbf{R}_h = \begin{bmatrix} \rho(0;0,0) & \rho(1;0,1) & \cdots & \rho(L-1;0,L-1) \\ \rho(1;1,0) & \rho(0;1,1) & \cdots & \rho(L-2;1,L-1) \\ \vdots & \vdots & \vdots & \vdots \\ \rho(L-1;L-1,0) & \rho(L-2;L-1,1) & \cdots & \rho(0;L-1,L-1) \end{bmatrix} \tag{12}$$

where $\mathbf{I}_{L_p}$ is an identity matrix of size $L_p \times L_p$. Thus, the system with colored Gaussian noise $\mathbf{z}_k$ is equivalently converted to a system with white Gaussian noise $\bar{\mathbf{z}}_k$, as described in (15).

It is well known that the error probability of the SIMO system with white Gaussian noise can be minimized by a maximal ratio combining (MRC) receiver [8]. With the system equation given in (15), the decision variable η_k at the output of the MRC receiver can be written as

$$\eta_k = \bar{\mathbf{h}}_k^H \bar{\mathbf{y}}_k = \mathbf{h}_k^H \mathbf{\Psi}_p \mathbf{y}_k \tag{17}$$

and the corresponding optimum detection rule is

$$\hat{x}(k) = \arg\min_{s_m \in \mathcal{S}} |\eta_k - q_k \cdot s_m|^2, \qquad \frac{k}{\nu} \text{ is integer} \tag{18}$$

where $\hat{x}(k)$ is the detected symbol at time instant k, $\mathcal{S}$ is the modulation alphabet set with cardinality M, the real-valued scalar $q_k = \mathbf{h}_k^H \mathbf{\Psi}_p \mathbf{h}_k$ is a quadratic form of the CGRV vector $\mathbf{h}_k$, and the Hermitian matrix $\mathbf{\Psi}_p$ is defined in (13) based on the nonzero eigenvalues of the colored noise covariance matrix $\mathbf{R}_z = N_0 \mathbf{R}_p$.

From (10) and (17), the decision variable η_k can be alternatively expressed as

$$\begin{aligned} \eta_k &= \mathbf{h}_k^H \mathbf{\Psi}_p \mathbf{h}_k \cdot x(k) + \mathbf{h}_k^H \mathbf{\Psi}_p \mathbf{z}_k \\ &= q_k \cdot x(k) + \mathbf{h}_k^H \mathbf{\Psi}_p \mathbf{z}_k. \end{aligned} \tag{19}$$

From (19), the instantaneous postdetection SNR at the output of the MRC receiver can be calculated as

$$\gamma_{\mathrm{MRC}} = \gamma \cdot q_k \tag{20}$$

where $q_k = \mathbf{h}_k^H \mathbf{\Psi}_p \mathbf{h}_k$, and $\gamma = E_s/N_0$ is the SNR without fading, with E_s being the average symbol energy.

Combining the decision rule described in (18) and the instantaneous postdetection SNR γ_{MRC} given in (20), we have the conditional error probabilities for m-ary amplitude-shift keying (MASK), square m-ary quadrature-amplitude modulation (MQAM), and m-ary phase-shift keying (MPSK) systems written as follows [8, eqs. (8.5), (8.12), and (8.23)]:

■ **MASK** :

$$P_{\mathrm{MASK}}(E|q_k) = \left(\frac{2}{\pi} - \frac{2}{\pi M}\right) \int_0^{\frac{\pi}{2}} \exp\left\{\frac{-3\gamma \cdot q_k}{(M^2-1)\sin^2\phi}\right\} d\phi \tag{21}$$

■ **MQAM** :

$$\begin{aligned} P_{\mathrm{MQAM}}(E|q_k) = &\left(\frac{4}{\pi} - \frac{4}{\pi\sqrt{M}}\right) \int_0^{\frac{\pi}{2}} \exp\left\{\frac{-3\gamma \cdot q_k}{2(M-1)\sin^2\phi}\right\} d\phi \\ &- \frac{4}{\pi}\left(1 - \frac{1}{\sqrt{M}}\right)^2 \int_0^{\frac{\pi}{4}} \exp\left\{\frac{-3\gamma \cdot q_k}{2(M-1)\sin^2\phi}\right\} d\phi \end{aligned} \tag{22}$$

TABLE I
PARAMETERS OF THE UNIFIED ERROR-PROBABILITY EXPRESSIONS

	ζ	β_1	$-\beta_2$	ψ_1	ψ_2
MASK	$\frac{3}{M^2-1}$	$(2-\frac{2}{M})$	0	$\frac{\pi}{2}$	0
MQAM	$\frac{3}{2(M-1)}$	$\left(4-\frac{4}{\sqrt{M}}\right)$	$\left(2-\frac{2}{\sqrt{M}}\right)^2$	$\frac{\pi}{2}$	$\frac{\pi}{4}$
MPSK	$\sin^2\frac{\pi}{M}$	1	0	$(\pi-\frac{\pi}{M})$	0

■ **MPSK** :

$$P_{\mathrm{MPSK}}(E|q_k) = \frac{1}{\pi} \int_0^{\pi - \frac{\pi}{M}} \exp\left\{-\frac{\gamma \cdot q_k \sin^2\left(\frac{\pi}{M}\right)}{\sin^2\phi}\right\} d\phi. \tag{23}$$

Equations (21)–(23) are the conditional error probabilities for the MASK, MQAM, and MPSK systems, respectively. Since all of the CEPs contain integrations with integrand in the form of an exponential function of $q_k = \mathbf{h}_k^H \mathbf{\Psi}_p \mathbf{h}_k$, the CEPs for the three modulated systems can be written in a unified form as follows:

$$P(E|q_k) = \sum_{i=1}^{2} \frac{\beta_i}{\pi} \int_0^{\psi_i} \exp\left\{-\zeta \cdot \frac{\gamma \cdot q_k}{\sin^2\theta}\right\} d\theta \tag{24}$$

where γ is the average SNR without fading, and the values of ζ, β_i, and ψ_i for the various modulation schemes are listed in Table I.

B. SER

The unconditional error probabilities $P(E)$ of the linearly modulated systems with colored noise and correlated Rayleigh fading channels are derived in this section with the help of the characteristic function (CHF) of the quadratic form of the CGRV vector.

For Rayleigh fading channels, the fading vector $\mathbf{h}_k$ is zero-mean Gaussian distributed with covariance matrix $\mathbf{R}_h$ given in (12), i.e., $\mathbf{h}_k \sim \mathcal{N}(0, \mathbf{R}_h)$. In the unified representation of the CEPs in (24), the integrands have the form of an exponential function of the real-valued random variable $q_k = \mathbf{h}_k^H \mathbf{\Psi}_p h_k$. Since $\mathbf{\Psi}_p$ is a Hermitian matrix, q_k is a quadratic form of the zero-mean CGRV vector $\mathbf{h}_k$, and the CHF of q_k is [22]

$$\Phi_q(w) = E(e^{jwq_k}) = [\det(\mathbf{I}_L - jw\mathbf{R}_h\mathbf{\Psi}_p)]^{-1} \tag{25}$$

where w is a dumb variable, and $\mathbf{I}_l$ is an $L \times L$ identity matrix.

With the CHF defined in (25) and the unified CEP $P(E|q_k)$ given in (24), the unconditional error probability $P(E) = E[P(E|q_k)]$ in Rayleigh fading channels can be computed as

$$\begin{aligned} P(E) &= \sum_{i=1}^{2} \frac{\beta_i}{\pi} \int_0^{\psi_i} \left[\det\left(\mathbf{I}_L + \frac{\zeta\gamma}{\sin^2\theta}\mathbf{R}_h\mathbf{\Psi}_p\right)\right]^{-1} d\theta \\ &= \sum_{i=1}^{2} \frac{\beta_i}{\pi} \int_0^{\psi_i} \left\{\det\left[\mathbf{I}_L + \frac{\zeta\gamma}{\sin^2\theta}\mathbf{\Psi}_p^{\frac{1}{2}}\mathbf{R}_h\left(\mathbf{\Psi}_p^{\frac{1}{2}}\right)^H\right]\right\}^{-1} d\theta \end{aligned} \tag{26}$$

where $\mathbf{\Psi}_p^{1/2}$ is the square root of the matrix Ψ_p satisfying $(\mathbf{\Psi}_p^{1/2})^H \mathbf{\Psi}_p^{1/2} = \mathbf{\Psi}_p$, and the identity $\det(\mathbf{I}+\mathbf{AB}) = \det(\mathbf{I}+\mathbf{BA})$ is used in (26).

Performing eigenvalue decomposition of the product matrix $\mathcal{R} = \mathbf{\Psi}_p^{1/2}\mathbf{R}_h(\mathbf{\Psi}_p^{1/2})^H$, we will have

$$\mathcal{R} = \mathbf{U}\mathbf{\Lambda}\mathbf{U}^H \tag{27}$$

where $\mathbf{\Lambda} = \mathrm{diag}[\lambda_1, \ldots, \lambda_{\tilde{L}}, 0, \ldots, 0] \in \mathbb{R}^{L\times L}$ is a diagonal matrix with the diagonal elements being the eigenvalues of $\mathcal{R}$, $\tilde{L}$ is the number of nonzero eigenvalues of $\mathcal{R}$, and the columns of the unitary matrix $\mathbf{U}$ are the corresponding orthonormal eigenvectors with $\mathbf{U}\mathbf{U}^H = \mathbf{I}_l$. The values of $\tilde{L}$ and λ_l, for $l = 1, 2, \ldots, \tilde{L}$, are determined by both $\mathbf{\Psi}_p$ and the temporal-delay correlation matrix $\mathbf{R}_h$, which are in turn related to the sampler timing offset and the statistical properties of the colored Gaussian noise and the doubly selective channel fading.

Substituting (27) into (26), we can write the symbol error probability as

$$\begin{aligned} P(E) &= \sum_{i=1}^{2} \frac{\beta_i}{\pi} \int_0^{\psi_i} \left\{ \det\left[\mathbf{U}\left(\mathbf{I}_L + \frac{\zeta\gamma}{\sin^2\theta}\mathbf{\Lambda} \right)\mathbf{U}^H \right] \right\}^{-1} d\theta \\ &= \sum_{i=1}^{2} \frac{\beta_i}{\pi} \int_0^{\psi_i} \prod_{l=1}^{\tilde{L}} \left[1 + \gamma \cdot \frac{\zeta\lambda_l}{\sin^2\theta} \right]^{-1} d\theta. \end{aligned} \tag{28}$$

The closed-form expressions of the SER given in (28) can be obtained by partial fraction expansion. For all systems with practical PDPs, e.g., the exponential profile [10] and the typical urban (TU) profile [21], the nonzero eigenvalues λ_l, for $l = 1, \ldots, \tilde{L}$ are different from each other, and the SER can be expressed as

$$P(E) = \sum_{i=1}^{2} \sum_{l=1}^{\tilde{L}} \frac{\beta_i d_l}{\pi} \int_0^{\psi_i} \left[1 + \gamma \cdot \frac{\zeta\lambda_l}{\sin^2\theta} \right]^{-1} d\theta \tag{29}$$

where the value of d_l can be computed by

$$d_l = \prod_{\substack{j=1 \\ j\neq l}}^{\tilde{L}} \frac{\lambda_l}{\lambda_j - \lambda_l}, \qquad \text{for } l = 1, 2, \ldots, \tilde{L}. \tag{30}$$

The integral in (29) can be expressed in closed form as follows:

$$\begin{aligned} &\frac{1}{\pi}\int_0^{\psi} \left[1 + \frac{\gamma\zeta\lambda_l}{\sin^2\theta} \right]^{-1} d\theta = \frac{\psi}{\pi} - \sqrt{\frac{\gamma\zeta\lambda_l}{1+\gamma\zeta\lambda_l}} \\ &\cdot \left[\frac{1}{2} - \frac{1}{\pi}\arctan\left(\sqrt{\frac{\gamma\zeta\lambda_l}{1+\gamma\zeta\lambda_l}}\cot\psi \right) \right] \qquad \forall \psi \in [0, 2\pi]. \end{aligned} \tag{31}$$

The derivation of (31) is outlined in the Appendix.

From (29)–(31), the unified closed-form SER solutions of the linearly modulated systems can be expressed by

$$\begin{aligned} P(E) = \sum_{i=1}^{2}\sum_{l=1}^{\tilde{L}} \beta_i d_l \Bigg\{ &\frac{\psi_i}{\pi} - \sqrt{\frac{\gamma\zeta\lambda_l}{1+\gamma\zeta\lambda_l}} \\ &\times \left[\frac{1}{2} - \frac{1}{\pi}\arctan\left(\sqrt{\frac{\gamma\zeta\lambda_l}{1+\gamma\zeta\lambda_l}}\cot\psi_i \right) \right] \Bigg\}. \end{aligned} \tag{32}$$

With the variables of ζ, β_i, and ψ_i in (32) substituted by the values given in Table I, the closed-form expressions of the SER lower bounds for MASK, MQAM, and MPSK systems with doubly selective channel fading can be written as (33)–(35), shown at the bottom of the page.

For the special case of frequency-flat fading channel, we have $\tilde{L} = 1$, and (34) and (35) agree with the exact error-probability expressions previously obtained in [20, eqs. (43) and (36)] for systems with flat fading channels.

In some special cases, such as the equal-gain T_{sym}-spaced PDP with the T_{sym}-spaced receiver, some of the eigenvalues of $\mathcal{R}$ may have identical values. To avoid the complexity of

---

■ **MASK** :

$$P_{\mathrm{MASK}}(E) = \sum_{l=1}^{\tilde{L}} d_l \left[\frac{M-1}{M}\left(1 - \sqrt{\frac{3\gamma\lambda_l}{M^2-1+3\gamma\lambda_l}} \right) \right] \tag{33}$$

■ **MQAM** :

$$\begin{aligned} P_{\mathrm{MQAM}}(E) = \sum_{l=1}^{\tilde{L}} d_l \Bigg\{ &\left(2 - \frac{2}{\sqrt{M}} \right)\left(1 - \sqrt{\frac{3\gamma\lambda_l}{3\gamma\lambda_l + 2M - 2}} \right) \\ &+ \left(1 - \frac{1}{\sqrt{M}} \right)^2 \left[\frac{4}{\pi}\sqrt{\frac{3\gamma\lambda_l}{3\gamma\lambda_l+2M-2}} \cdot \left(\frac{\pi}{2} - \arctan\sqrt{\frac{3\gamma\lambda_l}{3\gamma\lambda_l+2M-2}} \right) - 1 \right] \Bigg\} \end{aligned} \tag{34}$$

■ **MPSK** :

$$P_{\mathrm{MPSK}}(E) = \sum_{l=1}^{\tilde{L}} d_l \left\{ \frac{M-1}{M} - \sqrt{\frac{\gamma\lambda_l \sin^2\left(\frac{\pi}{M}\right)}{1+\gamma\lambda_l\sin^2\left(\frac{\pi}{M}\right)}} \left[\frac{1}{2} + \frac{1}{\pi}\arctan\left(\sqrt{\frac{\gamma\lambda_l\sin^2\left(\frac{\pi}{M}\right)}{1+\gamma\lambda_l\sin^2\left(\frac{\pi}{M}\right)}}\cot\left(\frac{\pi}{M}\right) \right) \right] \right\}. \tag{35}$$

partial fraction expansion of expressions with roots multiplicity, an approximation method is presented in [22], where identical eigenvalues are slightly modified without apparently affecting the system performance. By subtracting different small positive random numbers from identical eigenvalues, a valid error-probability lower bound can be obtained from (32). Moreover, exact values of $P(E)$ can still be computed from numerical integration of (28), which can be easily evaluated since it has finite integration limits and the integrand contains only elementary functions.

In the SER expressions given in (28) and (33)–(35), the effects of receiver oversampling, sampler timing offset τ_0, Doppler spread f_d, and PDP $G(\mu)$ of the physical channel fading are quantified as the eigenvalues of matrix $\mathcal{R}$, which is a function of the temporal-delay correlation matrix $\mathbf{R}_h$ and the matrix $\mathbf{\Psi}_p$.

For a system with binary modulation, i.e., $M = 2$, the SER presented in (33) has a similar expression as the matched filter bounds given in [11, eq. (11)] or [14, eq. (8)]. Nevertheless, the meaning of the eigenvalues used in (33) is quite different from those used in the conventional matched filter bounds in the literature. In this paper, the eigenvalues are jointly determined by the receiver sampling rate, sampler timing offset, and the effects of the physical fading, whereas the eigenvalues used by conventional matched filter bounds are determined by physical fading alone, and no effects of the sampler timing offset have been considered. It will be shown by simulations that the sampler timing offset has significant impact on the performance of the system with a symbol-spaced receiver.

V. Numerical Examples

Numerical examples are given in this section to illustrate the error performances of wireless communication systems with doubly selective fading channels, and simulation results are also provided to validate our analytical expressions.

In the examples, the symbol period is set to $T_{\rm sym} = 3.69\ \mu$s, and the maximum Doppler spread f_d is assumed to be 200 Hz, which corresponds to a mobile speed of 120 km/h at a carrier frequency of 1.8 GHz. Unless otherwise specified, a root-raised cosine (RRC) filter with a rolloff factor of $\alpha = 0.3$ is used as both the transmit and receive filters.

In the first example, we are going to compare our new analytical results with the well-known union Chernoff bounds and TUB [8]. Since the intertap correlation information will lead to "considerable analytical difficulty" [4] to obtain the union bounds, a simple two-ray equal-gain $T_{\rm sym}$-spaced PDP with uncorrelated channel gains are used in this example. The analytical results along with the corresponding simulation results obtained with MLSE and MAP equalizers are shown in Fig. 2. The decoding length of the equalizers is 1024 symbols, i.e., the equalizers are operated over 1024-symbol frames. Each point on the bit error rate curve is calculated based on 5000 frames. In the computation of the union bounds, the trellis structure of the system is analyzed based on the error state transition matrix method [3]. It is clear from the figure that our new performance results are superior to both of the two union bounds. The new SER lower bound can accurately predict the

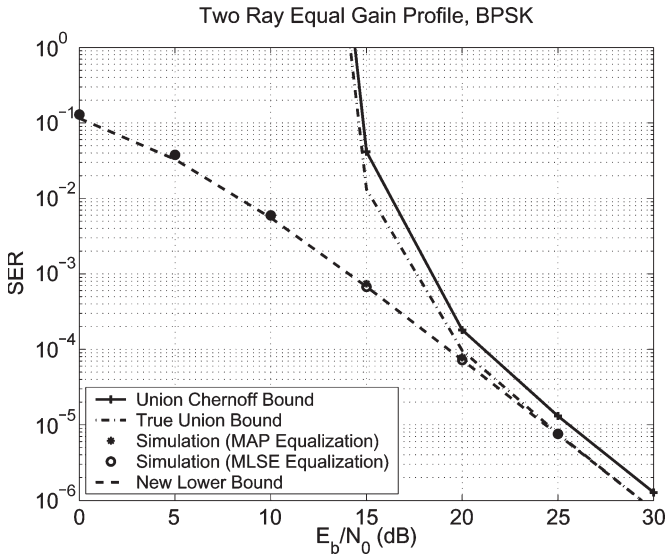

Fig. 2. Comparison of the performance bounds of systems with two-ray equal-gain channel profile (decoding length for the equalizers: 1024 symbols).

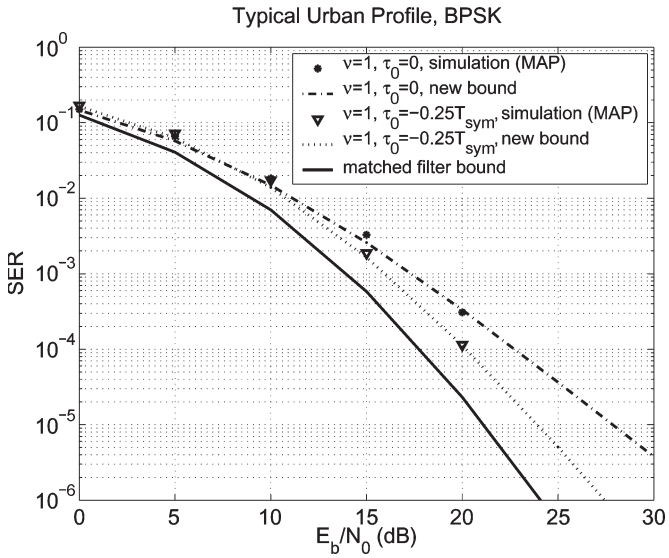

Fig. 3. Performances of systems with TU profile (ν: oversampling factor, τ_0: sampling timing offset, decoding length of the equalizers: 1024 symbols).

performances of MLSE and MAP equalizers at both low SNR and high SNR. On the other hand, the union Chernoff bound and TUB converge only when E_b/N_0 is higher than 20 dB. Even at high SNR, the union Chernoff bound is still 1 dB away from the actual error performances. Moreover, since the error probabilities of the newly proposed methods are analyzed on a symbol-by-symbol basis, considerable computation efforts can be saved compared to the trellis structure analysis used by the union bounds.

The performances of systems with practical PDPs are illustrated in the next example, and the TU profile [21] is used to model the frequency-selective channel fading. RRC filters with 100% excessive bandwidth $(\alpha = 1)$ are used as the transmit and receive filters. Fig. 3 shows the theoretical error performances as well as the simulation results obtained with the MAP equalizer, and the matched filter bound is also depicted in the figure for comparison purposes. From the figure,

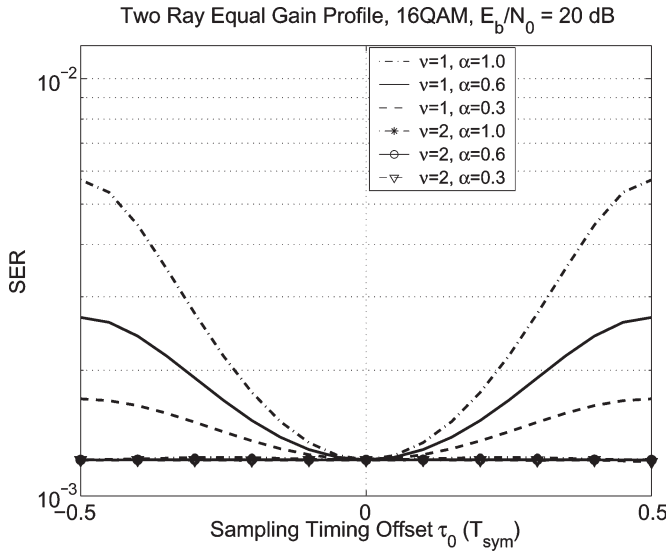

Fig. 4. Effects of sampler timing offset on system performance for two-ray equal-gain profile (ν: oversampling factor, τ_0: sampler timing offset, α: rolloff factor of the RRC filter).

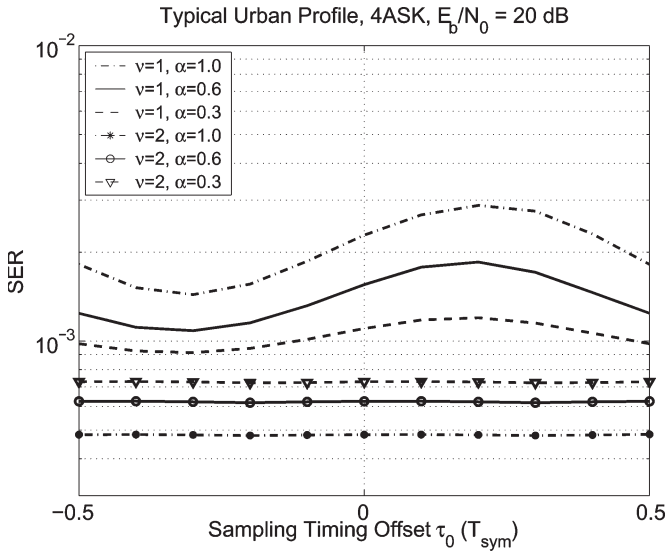

Fig. 5. Effects of sampler timing offset on system performance for TU profile (ν: oversampling factor, τ_0: sampling timing offset, α: rolloff factor of the RRC filter).

it is interesting to note that for systems without oversampling ($\nu = 1$), the performance of the system with sampler timing offset $\tau_0 = -0.25T_{\rm sym}$ is superior to that of the system with $\tau_0 = 0$. This phenomenon is due to the fact that the power of the TU profile is dominated by the delayed scattering rays of the physical channel fading, and the power of the first ray (or the zero-delay scattering ray) of the channel accounts for only 19.0% of the total channel power.

Moreover, excellent agreements between the simulation results and our new performance bounds can be observed from the figure for $E_b/N_0 \geq 10$ dB. The results in Figs. 2 and 3 show that the performances of MLSE and MAP equalizers coincide with the performance of interference-free systems at high SNR, which means that the residual ISI at the output of the MLSE and MAP equalizers tends to zero as the SNR tends to infinity. Thus, the MLSE and MAP equalizers are asymptotically optimum in the sense of interference cancellation. Even at low SNR, the lower bounds are still very tight compared to the simulation results. It can also be observed from Fig. 3 that the matched filter bound is a loose lower bound for such a system configuration. At an SER level of 10^{-5}, there is a 7-dB difference between the matched filter bound and the simulation results of systems with $\tau_0 = 0$. This difference is mainly induced by the ideal matched filter assumptions adopted in the derivation of the matched filter bound, and the effects of sampler timing offset cannot be represented by the matched filter bound either.

The effects of sampler timing phase and oversampling on system performance are further illustrated in the third example, where the SER lower bounds are plotted against the sampler timing offset τ_0 for systems with and without oversampling. Fig. 4 shows the performances of systems with the two-ray equal-gain uncorrelated $T_{\rm sym}$-spaced PDP, and the performances of systems with TU profile are displayed in Fig. 5. For systems without oversampling, i.e., $\nu = 1$, the system performances vary dramatically with the timing phase offset τ_0. This variation is induced by the effects of the spectrum aliasing of the received signals [17] since the sampling rate $1/T_{\rm sym}$ is smaller than the Nyquist rate $(1+\alpha)/T_{\rm sym}$ of the received signals, where α is the rolloff factor of the RRC filter. For different values of sampler timing phase, the amplitude of the overlapped spectrum could add up constructively or destructively, which will lead to performance improvement or degradation. The effects of spectrum aliasing become more serious for systems with larger excessive bandwidth (or larger value of α); thus, the performances of systems with larger α are more sensitive to the sampler timing offset. From Fig. 4, we can see that for systems with an equal-gain two-ray profile, the optimum sampler timing offset is $\tau_0 = 0$. However, for systems with TU profile, $\tau_0 = -0.3T_{\rm sym}$ is the optimum timing offset due to the power dominance of the delayed scattering rays of the channel fading.

As pointed out in [17], the timing phase sensitivity of the receiver can be avoided by oversampling. For systems with at most 100% excessive bandwidth, spectrum aliasing at the receiver can be completely removed by setting the oversampling factor $\nu = 2$. This statement is supported by our new performance bounds illustrated in Figs. 4 and 5, where the SERs for oversampled systems keep constant, regardless of the values of the sampler timing offset τ_0. For systems with TU profile, the performance of the oversampled system improves with the increase of the rolloff factor since more bandwidths are consumed by the signal, and there is no aliasing in the receiver.

So far, all of the examples are focused on systems with discrete-time PDPs, where the frequency-selective fading has discrete-time delayed multipaths. The analytical results proposed in this paper can also be directly applied to systems with continuous-time PDPs, such as the exponentially decaying PDP defined as $G(\mu) = A\exp(-\tau/T_{\rm sym})$, for $0 \leq \tau \leq 2T_{\rm sym}$, with A being a normalization factor. The timing phase sensitivity of systems with an exponentially decaying profile is shown in Fig. 6. From this figure, we can see that systems with an exponentially decaying profile have similar performances with

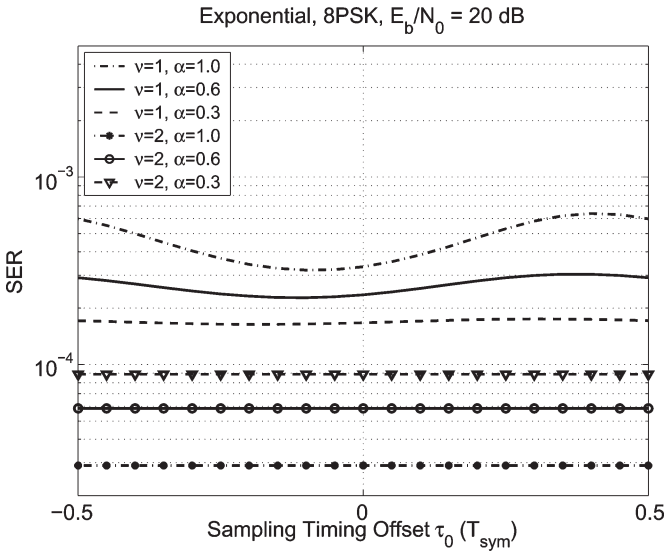

Fig. 6. Effects of sampler timing offset on system performance for the exponential decaying profile (ν: oversampling factor, τ_0: sampling timing offset, α: rolloff factor of the RRC filter).

the TU profile, and the optimum sampling timing offset for the exponentially decaying profile is $\tau_0 = -0.1T_{\rm sym}$.

VI. Conclusion

New and tight theoretical performance bounds were derived for wireless communication systems with time-varying and frequency-selective (i.e., doubly selective) channel fading and sampler timing offset. The SISO systems with doubly selective Rayleigh fading channels and fractionally spaced receivers were equivalently represented as a SIMO system with mutually *correlated* frequency-flat fading channels and colored Gaussian noise. Closed-form error-probability expressions were derived as lower bounds of symbol error probabilities for systems suffering both doubly selective channel fading and sampler timing offset. The information on timing phase offset, the statistical properties of channel fading, and the effects of the fractionally spaced receiver are quantified in the error-probability expressions.

Compared to the loose union bound and matched filter bound, our new analytical results can accurately predict the error performances of MLSE and MAP equalizers in practical system configurations at a wide range of SNR, and the results are obtained with a simple time-domain equivalent SIMO system method. Moreover, with the help of the theoretical expressions, the effects of receiver oversampling and timing phase sensitivity of communication systems are analyzed, and we have the following observations: 1) For systems with a symbol-spaced receiver and practical PDPs, zero sampler timing offset $(\tau = 0)$ is not always optimum. 2) For systems with at most 100% excessive bandwidth, two times symbol rate oversampling at the receiver can completely remove the phenomenon of timing phase sensitivity, which agrees with the theoretical analysis presented in [17]. 3) The timing phase sensitivity of a system with a symbol-spaced receiver becomes more serious with an increase in excessive system bandwidth.

Appendix
Derivation of (31)

The closed-form solution of the integral $1/\pi \int_0^{\psi}[1 + (a/\sin^2\theta)]^{-1}d\theta$, for $\psi \in [0, 2\pi]$, is derived here. Changing the integration variable to $z = \cot(\theta)$, we will have

$$\begin{aligned}\frac{1}{\pi}\int_0^{\psi}\Big[1+\frac{a}{\sin^2\theta}\Big]^{-1}d\theta &= \frac{1}{\pi}\int_{\cot\psi}^{+\infty}\big[(z^2+1)(az^2+a+1)\big]^{-1}dz \\ &= \frac{1}{\pi}\int_{\cot\psi}^{+\infty}(z^2+1)^{-1}dz \\ &\quad - \frac{1}{\pi}\int_{\cot\psi}^{+\infty}\left(z^2+\frac{a+1}{a}\right)^{-1}dz.\end{aligned} \tag{36}$$

The first integral of (36) can be evaluated as

$$\frac{1}{\pi}\int_{\cot\psi}^{+\infty}(z^2+1)^{-1}dz = \frac{1}{2} - \frac{1}{\pi}\arctan(\cot\psi) = \frac{\psi}{\pi} \tag{37}$$

where $\psi \in [0, 2\pi]$ is used in the second equality, and the second integral in (36) can be computed as

$$\begin{aligned}&\frac{1}{\pi}\int_{\cot\psi}^{+\infty}\left(z^2+\frac{a+1}{a}\right)^{-1}dz \\ &\quad= \frac{1}{\pi}\sqrt{\frac{a}{1+a}}\arctan\left(\sqrt{\frac{a}{1+a}}z\right)\Bigg|_{\cot\psi}^{+\infty} \\ &\quad= \sqrt{\frac{a}{1+a}}\left[\frac{1}{2} - \frac{1}{\pi}\arctan\left(\sqrt{\frac{a}{1+a}}\cot\psi\right)\right].\end{aligned} \tag{38}$$

Combining (36)–(38) leads to (31).

References

[1] G. D. Forney, Jr., "Maximum-likelihood sequence estimation of digital sequences in the presence of intersymbol interference," *IEEE Trans. Inf. Theory*, vol. IT-18, no. 3, pp. 363–378, May 1972.
[2] G. J. Foschini, "Performance bound for maximum-likelihood reception of digital data," *IEEE Trans. Inf. Theory*, vol. IT-21, no. 1, pp. 47–50, Jan. 1975.
[3] A. S. Acampora, "Analysis of maximum-likelihood sequence estimation performance for quadrature amplitude modulation," *Bell Syst. Tech. J.*, vol. 60, no. 4, pp. 865–885, Jul./Aug. 1981.
[4] G. L. Stuber, *Principles of Mobile Communication*, 2nd ed. Norwell, MA: Kluwer, 2001.
[5] B. D. Hart and D. P. Taylor, "Extended MLSE diversity receiver for the time- and frequency-selective channel," *IEEE Trans. Commun.*, vol. 45, no. 3, pp. 322–333, Mar. 1997.
[6] W.-H. Sheen and G. L. Stuber, "MLSE equalization and decoding for multipath-fading channels," *IEEE Trans. Commun.*, vol. 39, no. 10, pp. 1455–1464, Oct. 1991.
[7] W.-H. Sheen, C-C. Tseng, and C-S. Wang, "On the diversity, bandwidth, and performance of digital transmission over frequency-selective slow fading channels," *IEEE Trans. Veh. Technol.*, vol. 49, no. 3, pp. 835–843, May 2000.
[8] M. K. Simon and M.-S. Alouini, *Digital Communication Over Fading Channels*, 2nd ed. Hoboken, NJ: Wiley, 2005.

[9] J. E. Mazo, "Exact matched filter bound for two-beam Rayleigh fading," *IEEE Trans. Commun.*, vol. 39, no. 7, pp. 1027–1030, Jul. 1991.
[10] M. V. Clark, L. J. Greenstein, W. K. Kennedy, and M. Shafi, "Matched filter performance bounds for diversity combining receivers in digital mobile radio," *IEEE Trans. Veh. Technol.*, vol. 41, no. 4, pp. 356–362, Nov. 1992.
[11] V.-P. Kaasila and A. Mammela, "Bit error probability of a matched filter in a Rayleigh fading multipath channel," *IEEE Trans. Commun.*, vol. 42, no. 234, pp. 826–828, Feb.–Apr. 1994.
[12] T. Hunziker and D. Dahlhaus, "Bounds on matched filter performance in doubly dispersive Gaussian WSSUS channels," *Electron. Lett.*, vol. 37, no. 6, pp. 383–384, Mar. 2001.
[13] N. J. Baas and D. P. Taylor, "Matched filter bounds for wireless communication over Rayleigh fading dispersive channels," *IEEE Trans. Commun.*, vol. 49, no. 9, pp. 1525–1528, Sep. 2001.
[14] C. Schlegel, "Error probability calculation for multibeam Rayleigh channels," *IEEE Trans. Commun.*, vol. 44, no. 3, pp. 290–293, Mar. 1996.
[15] S.-C. Lin, "Accurate error rate estimate using moment method for optimum diversity combining and MMSE equalisation in digital cellular mobile radio," *Proc. Inst. Electr. Eng. Commun.*, vol. 149, no. 3, pp. 157–165, Jun. 2002.
[16] G. Ungerboeck, "Fractional tap-spacing equalizer and consequences for clock recovery in data modems," *IEEE Trans. Commun.*, vol. COM-24, no. 8, pp. 856–864, Aug. 1976.
[17] S. U. H. Qureshi, "Adaptive equalization," *Proc. IEEE*, vol. 73, no. 9, pp. 1349–1387, Sep. 1985.
[18] C. Xiao, J. Wu, S. Y. Leong, Y. R. Zheng, and K. B. Letaief, "A discrete-time model for triply selective MIMO Rayleigh fading channels," *IEEE Trans. Wireless Commun.*, vol. 3, no. 5, pp. 1678–1688, Sep. 2004.
[19] C. Sgraja and C. Xiao, "On discrete-time modeling of time-varying WSSUS fading channels," in *Proc. IEEE ICC*, Istanbul, Turkey, Jun. 11–15, 2006, pp. 5486–5490.
[20] M. G. Shayesteh and A. Aghamohammadi, "On the error probability of linearly modulated signals on frequency-flat Ricean, Rayleigh, and AWGN channels," *IEEE Trans. Commun.*, vol. 43, no. 234, pp. 1454–1466, Feb.–Apr. 1995.
[21] *Radio Transmission and Reception*, Nov. 2000. ETSI. GSM 05.05. ETSI EN 300 910 V8.5.1.
[22] S. Siwamogsatham, M. P. Fitz, and J. H. Grimm, "A new view of performance analysis of transmit diversity schemes in correlated fading," *IEEE Trans. Inf. Theory*, vol. 48, no. 4, pp. 950–956, Apr. 2002.
[23] G. E. Bottomley and S. Chennakeshu, "Unification of MLSE receivers and extension to time-varying channels," *IEEE Trans. Commun.*, vol. 46, no. 4, pp. 464–472, Apr. 1998.
[24] A. Papoulis and S. U. Pillai, *Probability, Random Variables and Stochastic Processes*, 4th ed. New York: McGraw-Hill, 2002.

Jingxian Wu (S'02–M'06) received the B.S. degree from the Beijing University of Aeronautics and Astronautics, Beijing, China, in 1998, the M.S. degree from Tsinghua University, Beijing, in 2001, and the Ph.D. degree from the University of Missouri-Columbia, in 2005, all in electrical engineering.

He is currently an Assistant Professor at the Department of Engineering Science, Sonoma State University, Rohnert Park, CA. His research interests include the physical layer of wireless communication systems, including error performance analysis, space-time coding, channel estimation and equalization, and spread-spectrum communications.

Dr. Wu is a member of Tau Beta Pi. He is a Technical Program Committee Member for the 2006 IEEE Global Telecommunications Conference, the 2007 IEEE Wireless Communications and Networking Conference, and the 2007 IEEE International Conference on Communications.

Chengshan Xiao (M'99–SM'02) received the B.S. degree from the University of Electronic Science and Technology of China, Chengdu, China, in 1987, the M.S. degree from Tsinghua University, Beijing, China, in 1989, and the Ph.D. degree from the University of Sydney, Sydney, Australia, in 1997, all in electrical engineering.

From 1989 to 1993, he was a member of the Research Staff and then became a Lecturer at the Department of Electronic Engineering, Tsinghua University. From 1997 to 1999, he was a Senior Member of Scientific Staff at Nortel Networks, Ottawa, ON, Canada. From 1999 to 2000, he was a Faculty Member at the Department of Electrical and Computer Engineering, University of Alberta, Edmonton, AB, Canada. Since 2000, he has been with the Department of Electrical and Computer Engineering, University of Missouri-Columbia, where he is currently an Associate Professor. He holds three U.S. patents in wireless communications area. His algorithms have been implemented into Nortel's base station radios with successful technical field trials and network integration. His research interests include wireless communication networks and signal processing, and he has published extensively in these areas.

Dr. Xiao is currently the founding Area Editor for Transmission Technology of the IEEE TRANSACTIONS ON WIRELESS COMMUNICATIONS. Previously, he was an Associate Editor for the IEEE TRANSACTIONS ON VEHICULAR TECHNOLOGY, the IEEE TRANSACTIONS ON CIRCUITS AND SYSTEMS I, and the international journal *Multidimensional Systems and Signal Processing*. He has been involved in organizing major international conferences. These include serving as a Program Co-Chair for the 2007 IEEE Wireless Communications and Networking Conference and Vice Chair for the 2005 IEEE Globecom Wireless Communications Symposium. He has also served as a Technical Program Committee Member for a number of IEEE international conferences, including ICC, Globecom, and WCNC in the last few years. He is currently the Chair of the IEEE Communications Society Technical Committee on Personal Communications and a member of the IEEE Communications Society Technical Activity Council.